



Subsurface Charge Repulsion of Adsorbed H-Adatoms on TiO₂(110)

Jo Onoda,[†] Chi Lun Pang,^{*,‡} Ayhan Yurtsever,^{*,†,§} and Yoshiaki Sugimoto[†]

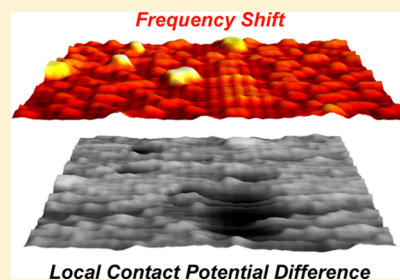
[†]Graduate School of Engineering, Osaka University, 2-1 Yamada-Oka, Suita, Osaka 565-0871, Japan

[‡]Department of Chemistry and London Centre for Nanotechnology, University College London, London WC1H 0AJ, United Kingdom

[§]Institute of Scientific and Industrial Research, Osaka University, 8-1 Mihogaoka, Ibaraki, Osaka 567-0047, Japan

Web-Enhanced Feature

ABSTRACT: We have used noncontact atomic force microscopy (NC-AFM) and Kelvin probe force microscopy (KPFM) to directly visualize the presence of charged subsurface impurities on rutile TiO₂(110). The subsurface charges add an additional electrostatic force between the sample and tip so that they appear as hillocks in the NC-AFM topography. Analysis of several subsurface defects in the same NC-AFM image reveals that the hillocks have discrete heights, which means that defects at different subsurface levels can be detected and distinguished. H adatoms, which are positively charged at the TiO₂(110) surface, were found to be repelled by the buried positive charge, so that they form a ~80–120 Å wide hydrogen-free zone around the charge. Thus, there is an opportunity to deliberately add dopants in order to exclude or perhaps even to confine certain adsorbates to a local region at the surface.



INTRODUCTION

TiO₂ has been investigated intensely since the 1970s when it was discovered that it is an active photocatalyst.¹ However, the relatively large band gap of TiO₂ means that it is mainly responsive to the ultraviolet spectrum. Since then, a line of research has focused on finding appropriate dopants to add to the titania to make it photoactive with visible light.² Most surface science studies focus on the most thermodynamically stable rutile TiO₂(110) face,^{3,4} and naturally, this surface has been used to examine the role that dopants play in catalysis.^{5–8}

It is becoming more and more apparent that both extrinsic subsurface dopants and intrinsic subsurface defects can dramatically modify the behavior at the surface.^{9–14} For instance, exposing the rutile TiO₂(110) surface to O₂ and then annealing in ultrahigh vacuum (UHV) or simply annealing TiO₂(110) in a partial pressure of O₂ leads to the creation of TiO_x ($x < 2$) islands because of segregation and subsequent reaction of interstitial Ti with oxygen.^{9,12,13} On the other hand, when TiO₂(110) is doped with niobium, Nb can also occupy interstitial sites and thereby suppress the formation of TiO_x.¹²

Nb-doped TiO₂(110) has received particular attention in part because it can be used to introduce conductivity to TiO₂(110) thus enabling charged-particle techniques such as scanning tunneling microscopy (STM) and low-energy electron diffraction (LEED) to be employed easily. At densities of ~1 wt % Nb, LEED and STM images appear the same as undoped (but bulk-reduced) TiO₂(110) with the exception of some bright spots in the STM image which are assigned to Ti neighboring with Nb.¹⁵ However, at doping levels of ~0.05 wt % Nb, even on the atomic scale, STM images are indistinguishable from undoped TiO₂(110).¹⁶

Here, we use noncontact atomic force microscopy (NC-AFM) and Kelvin probe force microscopy (KPFM) to study subsurface charges and their effect on the adsorption of H adatoms on 0.05 wt % Nb-doped rutile TiO₂(110). KPFM measurements show that charged species are present beneath the surface and are manifested as bright regions in NC-AFM. These charged regions, which are assigned to single positively charged ions, repel the positively charged H adatoms that normally decorate the surface. Charged subsurface dopants may therefore be exploited as a means of restricting certain charged adsorbates from parts of the surface, and perhaps other adsorbates could even be confined in those regions.

EXPERIMENTAL METHODS

The experiments were performed in Osaka using an ultrahigh-vacuum chamber (with a base pressure of $\sim 5 \times 10^{-11}$ Torr) which contains a custom-built NC-AFM that was operated at room temperature. The 0.05 wt % Nb-doped TiO₂(110) crystal (Shinko-sha) was prepared using repeated cycles of Ar-ion bombardment (2 keV) for approximately 5 min and annealing (1100 K) for 10 min.

The NC-AFM was operated using the frequency modulation detection method¹⁷ with the cantilever oscillation amplitude kept constant (peak-to-peak amplitude 105 Å). The conductive silicon cantilever had a resonant frequency of 164.55 kHz. All images except for those in Figure 3 were obtained in the constant frequency shift (Δf) mode.

Received: April 7, 2014

Revised: May 8, 2014

Published: May 12, 2014

KPFM measurements were conducted in the frequency modulation mode whereby an ac voltage ($U_{\text{ac,rms}} = 0.5$ V, frequency $f_{\text{ac}} = 500$ Hz) and a dc bias voltage (V_{CPD}) were applied to the sample with the tip grounded. The dc bias is the voltage applied to compensate the local contact potential difference (LCPD).^{18–22}

All NC-AFM images presented here were recorded with this additional V_{CPD} , but the Kelvin contrast is only optimized for the image in Figure 3. This is evident by the charged patches only appearing faintly brighter in the Δf image in Figure 3 compared with the other NC-AFM topographic images. Furthermore, in the case of Figure 3 but not in the other images, crosstalk between the NC-AFM topography and the LCPD map was eliminated by using retrace scanning in constant height mode²² with the aid of a commercial scan controller.²³

RESULTS AND DISCUSSION

Subsurface Charges. Figure 1 shows a model of the $\text{TiO}_2(110)$ surface. The surface is characterized by rows of 5-

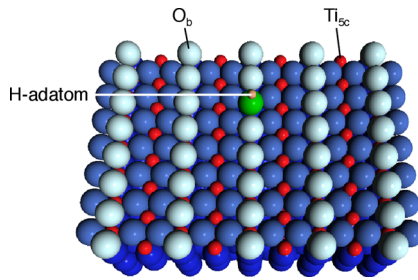


Figure 1. Ball model of $\text{TiO}_2(110)$. Small, red spheres denote Ti, and large, blue spheres denote O. O atoms nearer the surface are shaded lighter so that O_b species have the lightest shading. One O_b atom, shaded green, has a H adatom attached which is shaded pink.

fold coordinated Ti (Ti_{5c}) that alternate with rows of bridging O (O_b). Removal of O_b species during sample preparation leads to the formation of bridging oxygen vacancies ($\text{O}_b\text{-vac}$) which themselves react further with water from the residual vacuum to form two H adatoms per $\text{O}_b\text{-vac}$.^{24–26}

Figure 2 shows NC-AFM images of the Nb-doped $\text{TiO}_2(110)$ sample after it was prepared by sputter/anneal cycles and then was subsequently left to hydroxylate in the residual vacuum. In NC-AFM images, depending on the exact nature of the tip apex, Ti_{5c} rows can appear bright or dark as can point defects (i.e., $\text{O}_b\text{-vacs}$ or H adatoms).^{27–32} In the image shown in Figure 2a, the O_b rows are imaged bright and the H adatoms appear as dark depressions on those rows. In Figure 2b and c (and in all other images presented here), the contrast is inverted: Ti_{5c} rows are imaged bright and the H adatoms appear as bright spots between these Ti_{5c} rows. The images in Figure 2 are indistinguishable from those of pure $\text{TiO}_2(110)$ except for the presence of oval, bright patches.

Similar bright patches have previously been observed in empty-state STM images of undoped $\text{TiO}_2(110)$,^{10,11,24,26,33,34} but are only explicitly discussed by Batzill and co-workers^{10,33} and Ishida and Fujita,¹¹ as well as in review articles.^{35,36} Batzill et al.³³ attribute each bright region to a single positively charged subsurface defect by comparison with studies on doped semiconductor surfaces, such as GaAs and InP: positively charged *n*-type dopants appear bright in empty-state STM images.^{37–39} On the basis of time-of-flight secondary ion mass

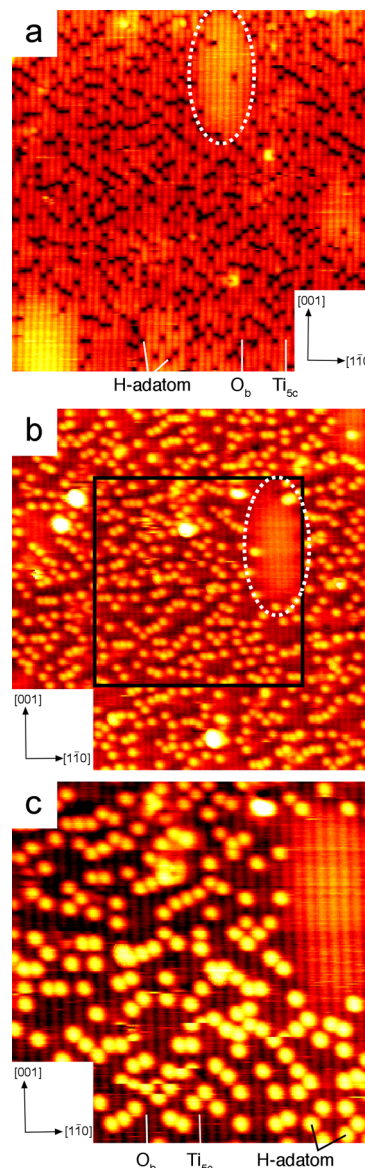


Figure 2. NC-AFM images of Nb-doped $\text{TiO}_2(110)$. (a) $(350 \text{ \AA})^2$, $\Delta f = -6.3$ Hz. Bright rows which run in the $[001]$ direction correspond to O_b rows, and the dark defects on these rows are H adatoms that arise from water dissociation in $\text{O}_b\text{-vacs}$.^{24–26} (b) $(350 \text{ \AA})^2$, $\Delta f = -5.7$ Hz. (c) $(200 \text{ \AA})^2$, $\Delta f = -5.7$ Hz. The square in b marks the approximate area of the image in c. In both b and c, bright rows correspond to Ti_{5c} rows and bright defects that appear between them are H adatoms. In all three images, bright patches can be observed, and examples are highlighted with dotted ovals in a and b. Additionally, in a and c examples of H adatoms, Ti_{5c} rows and O_b rows are highlighted.

spectroscopy, Batzill et al.³³ tentatively assigned the bright regions to subsurface vanadium (V^{5+}). Ishida and Fujita also assign the bright regions to subsurface positively charged ions but instead suggest that they are interstitial Ti ions.¹¹ Similar bright patches have also been observed in the NC-AFM topography of $\text{TiO}_2(110)$ ²⁹ as well as in STM images of $\text{ZnO}(000\bar{1})-\text{O}$ ^{40,41} and $\text{CaO}(001)$.⁴² In the cases of $\text{ZnO}(000\bar{1})-\text{O}$ and $\text{CaO}(001)$, the charge could even be manipulated by the STM.^{41,42}

KPFM enables measurement of the local contact potential difference (LCPD) simultaneously with NC-AFM, so that

charged regions of a surface are easily detected, showing up as bright or dark features in LCPD maps.^{18–22}

Figure 3 shows two images of the Nb-doped TiO₂(110) surface that were recorded simultaneously in the constant

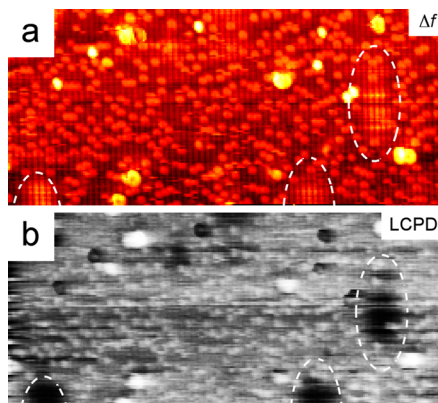


Figure 3. KPFM images ($475 \times 210 \text{ \AA}^2$) of Nb-doped TiO₂(110) recorded in constant height mode with mean $\Delta f = -8.2 \text{ Hz}$. (a) Δf map. (b) Local contact potential difference (LCPD) map. In both images, three charged regions are marked with part of white, dashed ovals. In the LCPD map, these charged regions appear dark indicating that they correspond to charged regions.

height mode. The constant height mode was used in order to eliminate any crosstalk between the NC-AFM topography and the LCPD signals.²² Figure 3a shows a map of Δf which corresponds to the NC-AFM image, whereas Figure 3b shows the LCPD map. Three bright regions are visible in the Δf map (Figure 3a) similar to those shown in Figure 2. These same regions that appear bright in the Δf image are dark in the corresponding LCPD map, indicating that they originate from subsurface charges. The subsurface charges probably originate from impurities like V⁵⁺, as suggested by Batzill et al.,³³ although given that the sample is deliberately doped with Nb, Nb⁵⁺ is also a possibility. Subsurface interstitial Ti ions as suggested by Ishida and Fujita¹¹ seem to be a less likely origin because these charged regions are known to appear only with certain crystals,³³ whereas interstitial Ti ions are always present.^{4,9,13,35,36}

The appearance of the charged regions as bright patches in the NC-AFM images of Figure 2 can be explained by the additional attractive force exerted on the tip by the subsurface charge that means the tip has to retract in order to maintain a constant Δf . As a result, the charged regions appear as hillocks in the NC-AFM topography.

Figure 4 shows an NC-AFM image together with line profiles from six charged regions, labeled i–vi. The line profiles are taken through the centers of each region in the [1̄10] and [001] directions. We observed several characteristics of the charged regions not previously reported. In each region, the extent of the hillock is greater in the [001] direction than in the [1̄10] direction. This, presumably, is related to the anisotropy of the dielectric constant. The crystal anisotropy also plays important roles in charge transport⁴³ and adsorbate diffusion⁴⁴ for which the [001] direction is the easy direction. Although each region appears to have a different lateral size in the image in Figure 4a, this is not borne out by the line profiles. In each line profile, the charged regions extend about 80 Å in [1̄10] and 120 Å in [001]. The charged regions also have discrete apparent heights in the NC-AFM image: either ~0.5 Å (i, iii, v) or ~0.9 Å (ii, iv,

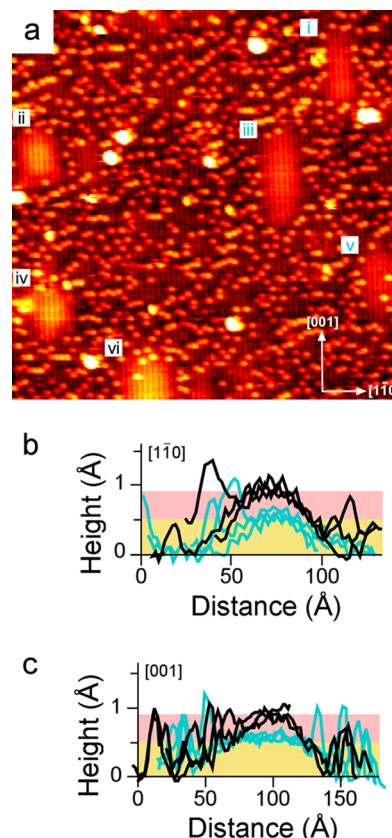


Figure 4. (a) A (475 \AA)² NC-AFM image ($\Delta f = -7.7 \text{ Hz}$) of Nb-doped TiO₂(110) showing six charged regions labeled i–vi. (b, c) The accompanying line profiles taken along [1̄10] in b and along [001] in c. Regions i, iii, v are labeled turquoise, and their line profiles are shown turquoise, whereas regions ii, iv, and vi are labeled in black and correspond to the black line profiles. The heights have discrete values: either ~0.5 Å (turquoise) or ~0.9 Å (black) as highlighted by the yellow and pink rectangles. The discrete heights correspond to charged defects at two different depths in the subsurface.

vi) as shown in the line profiles in Figure 4b and c. As with the conclusions from the STM measurements of Si dopants in GaAs,³⁸ we assign the regions with a greater apparent height to charged dopants nearer to the surface. The reason for our assignment is that a subsurface charge nearer to the surface will exert a greater force on the tip than a deeper-lying charge, and so it follows that for a charge nearer the surface, the tip has to retract further in order to maintain a constant Δf .

Inclusion of H Adatoms from the Charged Regions. It is rather striking in Figures 2–4 that H adatoms do not appear in the charged regions. Although no mechanism is proposed, Enevoldsen et al.²⁸ note that both in their NC-AFM images and in STM images from the literature [for example, Figure 2 in ref 26], H adatoms are excluded from positively charged regions on the TiO₂(110) surface.

In other work, Cl was deposited on TiO₂(110) and was also found to be excluded from a similarly, positively charged region.¹⁰ Upon deposition of Cl, the band gap state (BGS)⁴⁵ visible in valence band photoemission spectra of the clean surface is depleted, indicative of electron-charge transfer from the defects to the Cl.⁴⁶ Furthermore, there is a rigid shift of states to lower binding energy which is due to upward band-bending. Together, this indicates that Cl is negatively charged at the TiO₂(110) surface. Thus, it was proposed that the Cl

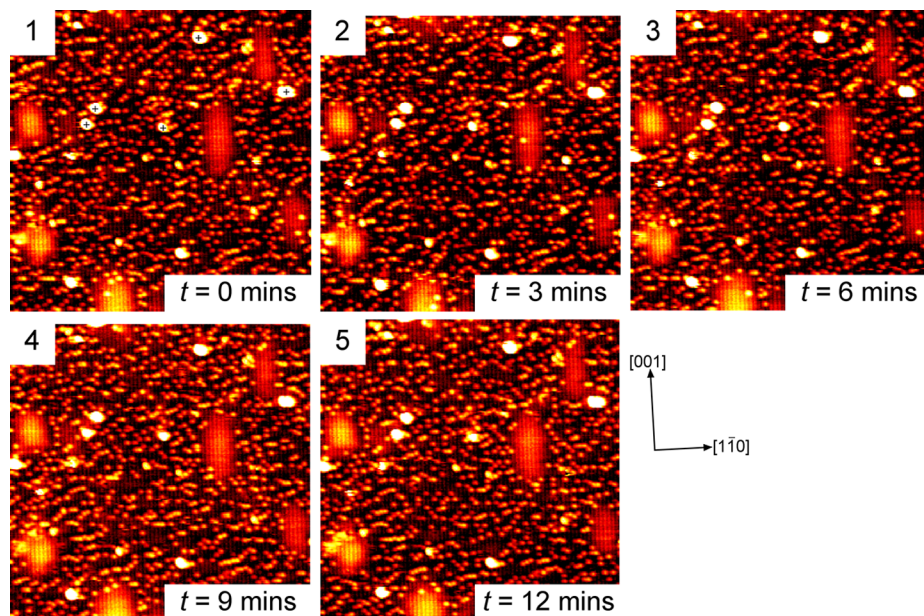


Figure 5. Five sequentially recorded (475 \AA) 2 NC-AFM images ($\Delta f = -7.7 \text{ Hz}$) of Nb-doped $\text{TiO}_2(110)$. Each frame takes ~ 3 min to record, and we set $t = 0$ in frame 1. Frame 1 is the same image as that in Figure 4. A small number of unidentified impurities are marked with black crosses in frame 1. This movie and another one with a smaller frame size are available as web-enhanced objects in MPEG format: Movie 1 and Movie 2.

atoms do not adsorb in the positively charged regions because of a competition for electrons between the Cl and the positively charged impurity atom.

It is known that H adatoms are mobile at room temperature, diffusing intrinsically along the [001] rows and across them by exchange with water.^{25,29,44} Thus, by recording the same area repeatedly, we can probe the behavior of these H adatoms dynamically. A sequence of five NC-AFM images of the same area is shown in Figure 5. A movie of this sequence as well as another sequence of six NC-AFM images is available as web-enhanced objects. Frame 1 in Figure 5 is the same image as that displayed in Figure 4, and we refer to each charged region (i–vi) in the same way. In frame 1 ($t = 0$), no H adatoms can be seen in region iii. However, in frame 2 ($t = 3 \text{ min}$), a H adatom appears before diffusing away by frame 3 ($t = 6 \text{ min}$). Although it appears as if the H adatom in the charged region is brighter than those outside, once the hillock is removed from the line profiles, this is not the case. A H adatom also appears in region i of frame 2 ($t = 3 \text{ min}$), remains present in frame 3 ($t = 6 \text{ min}$), but has diffused away by frame 4 ($t = 9 \text{ min}$). In these movies, the typical residency time for H adatoms at the positively charged regions was less than 3–6 min, and the maximum observed residency was less than 13 min.

A recent study demonstrates clearly that the BGS visible in valence band photoemission spectra of the clean surface is increased when H adatoms are adsorbed on O_b .⁴⁷ This is indicative of an electron-charge transfer from the H adatoms to TiO_2 , which leaves positively charged H adatoms at the surface. As such, the reason why H adatoms are excluded from the vicinity of the charged regions must be different from the case of Cl. A straightforward explanation for why the H adatoms tend not to reside in the vicinity of the charge regions is because they are repelled by the positive charge. Our time-lapse measurements shown in Figure 5 and the movies (available as web-enhanced objects) indicate that while the Coulomb repulsion disfavors H adsorption in the charged region, it is not completely prevented.

It is clear that for different reasons, both positively and negatively charged adsorbates can be excluded from the vicinity of the charged regions. However, this does not mean that all adsorbates are excluded from these charged regions, merely that there is a term that either lowers their adsorption energy or increases (decreases) the diffusion barrier into (out of) the region. For more strongly chemisorbed species such as carboxylic acids (and related molecules),^{48,49} the situation is likely to be different. Dosing carboxylic acids onto $\text{TiO}_2(110)$ generally leads to dissociative adsorption, whereby a (2×1) overlayer of the carboxylate (for instance, trimethyl acetic acetate (TMAA) in the case of trimethyl acetic acid) forms at $\text{Ti}_{\text{S}\zeta}$ sites along with the adsorption of H adatoms on O_b .^{3,4,35,36,48} In the STM image in Figure 5a of ref 48, some charged regions appear to be present, but it can be seen that TMAA is nevertheless adsorbed at those regions. As such, these charged regions may be used to locally separate coadsorbates. Furthermore, while H adatoms seem to be excluded from both shallower and deeper charges (see, for example, Figure 4), it was noted by Ishida and Fujita that some charged regions exclude Co-phthalocyanine whereas some did not.¹¹ This could be related to the depth of the charge.

CONCLUSIONS

In conclusion, we have unambiguously identified the presence of charged subsurface defects using KPFM. In NC-AFM, these charged areas appear as hillocks because of an additional electrostatic force. Analysis of several subsurface defects in the same NC-AFM image reveals that the hillocks have discrete heights, indicating that charged defects at distinct depths can be detected at the surface and distinguished. H adatoms, which are positively charged at the $\text{TiO}_2(110)$ surface, were found to be repelled by the buried positive charge, although sequential NC-AFM images of the same area show that the H adatoms can still reside transiently at the charged regions.

■ ASSOCIATED CONTENT

Web-Enhanced Feature

Movies of NC-AFM images are available in the HTML version of the paper.

■ AUTHOR INFORMATION

Corresponding Authors

*Tel: +44-207-679-5580. Fax: +44-207-679-0595. E-mail: chi.pang@ucl.ac.uk.

*Tel: +81-6-6879-7763. Fax: +81-6-6879-7764. E-mail: ayhan@afm.eei.eng.osaka-u.ac.jp.

Notes

The authors declare no competing financial interest.

■ ACKNOWLEDGMENTS

This work was supported by a Grant-in-Aid for Scientific Research (20760024, 26110516, 26600015) from the Ministry of Education, Culture, Sports, Science, and Technology of Japan (MEXT), Funding Program for Next Generation World-Leading Researchers, and Osaka University Visiting Scholar Program.

■ REFERENCES

- (1) Fujishima, A.; Honda, K. Electrochemical Photolysis of Water at a Semiconductor Electrode. *Nature (London)* **1972**, *238*, 37–38.
- (2) Chen, X.; Mao, S. S. Titanium Dioxide Nanomaterials: Synthesis, Properties, Modifications, and Applications. *Chem. Rev.* **2007**, *107*, 2891–2959.
- (3) Diebold, U. The Surface Science of Titanium Dioxide. *Surf. Sci. Rep.* **2003**, *48*, 53–229.
- (4) Pang, C. L.; Lindsay, R.; Thornton, G. Chemical Reactions on Rutile TiO₂(110). *Chem. Soc. Rev.* **2008**, *37*, 2328–2353.
- (5) Bechstein, R.; Kitta, M.; Schütte, J.; Kühnle, A.; Onishi, H. Surface Reconstruction Induced by Transition Metal Doping of Rutile Titanium Dioxide (110). *J. Phys. Chem. C* **2009**, *113*, 13199–13203.
- (6) Di Valentin, C.; Pacchioni, G.; Onishi, H.; Kudo, A. Cr/Sb Co-Doped TiO₂ from First Principles Calculations. *Chem. Phys. Lett.* **2009**, *469*, 166–171.
- (7) Mangham, A. N.; Govind, N.; Bowden, M. E.; Shutthanandan, V.; Joly, A. G.; Henderson, M. A.; Chambers, S. A. Photochemical Properties, Composition, and Structure in Molecular Beam Epitaxy Grown Fe “Doped” and (Fe,N) Codoped Rutile TiO₂(110). *J. Phys. Chem. C* **2011**, *115*, 15416–15424.
- (8) Batzill, M.; Morales, E. H.; Diebold, U. Influence of Nitrogen Doping on the Defect Formation and Surface Properties of TiO₂ Rutile and Anatase. *Phys. Rev. Lett.* **2006**, *96*, 026103.
- (9) Wendt, S.; Sprunger, P. T.; Lira, E.; Madsen, G. K. H.; Li, Z.; Hansen, J. Ø.; Matthiesen, J.; Blekinge-Rasmussen, A.; Laegsgaard, E.; Hammer, B.; et al. The Role of Interstitial Sites in the Ti3d Defect State in the Band Gap of Titania. *Science* **2008**, *320*, 1755–1759.
- (10) Batzill, M.; Hebenstreit, E. L. D.; Hebenstreit, W.; Diebold, U. Influence of Subsurface, Charged Impurities on the Adsorption of Chlorine at TiO₂(1 1 0). *Chem. Phys. Lett.* **2003**, *367*, 319–323.
- (11) Ishida, N.; Fujita, D. Adsorption of Co-Phthalocyanine on the Rutile TiO₂(110) Surface: A Scanning Tunneling Microscopy/Spectroscopy Study. *J. Phys. Chem. C* **2012**, *116*, 20300–20305.
- (12) Sasahara, A.; Tomitori, M. XPS and STM Study of Nb-Doped TiO₂(110)-(1 × 1) Surfaces. *J. Phys. Chem. C* **2013**, *117*, 17680–17686.
- (13) Smith, R. D.; Bennett, R. A.; Bowker, M. Measurement of the Surface-Growth Kinetics of Reduced TiO₂(110) during Reoxidation using Time-Resolved Scanning Tunneling Microscopy. *Phys. Rev. B* **2002**, *66*, 035409.
- (14) Torbrügge, S.; Reichling, M.; Ishiyama, A.; Morita, S.; Custance, Ó. Evidence of Subsurface Oxygen Vacancy Ordering on Reduced CeO₂(111). *Phys. Rev. Lett.* **2007**, *99*, 056101.
- (15) Morris, D.; Dou, Y.; Rebane, J.; Mitchell, C. E. J.; Eg dell, R. G.; Law, D. S. L.; Vittadini, A.; Casarin, M. Photoemission and STM Study of the Electronic Structure of Nb-Doped TiO₂. *Phys. Rev. B* **2000**, *61*, 13445–13457.
- (16) Shimizu, R.; Hitosugi, T.; Nakayama, K. S.; Sakurai, T.; Shiraiwa, M.; Hasegawa, T.; Hashizume, T. Preparation of Atomically Flat TiO₂(110) Substrate. *Jpn. J. Appl. Phys.* **2009**, *48*, 125506.
- (17) Albrecht, T. R.; Grütter, P.; Horne, D.; Rugar, D. Frequency Modulation Detection using High-Q Cantilevers for Enhanced Force Microscope Sensitivity. *J. Appl. Phys.* **1991**, *69*, 668–673.
- (18) Chung, H. J.; Yurtsever, A.; Sugimoto, Y.; Abe, M.; Morita, S. Kelvin Probe Force Microscopy Characterization of TiO₂(110)-supported Au Clusters. *Appl. Phys. Lett.* **2011**, *99*, 123102.
- (19) Barth, C.; Henry, C. R. Surface Double Layer on (001) Surfaces of Alkali Halide Crystals: A Scanning Force Microscopy Study. *Phys. Rev. Lett.* **2007**, *98*, 136804.
- (20) Sasahara, A.; Uetsuka, H.; Onishi, H. Individual Na Adatoms on TiO₂(110)-(1 × 1) Surface Observed Using Kelvin Probe Force Microscope. *Jpn. J. Appl. Phys.* **2004**, *43*, 4647–4650.
- (21) Neff, J. L.; Milde, P.; León, C. P.; Kundrat, M. D.; Eng, L. M.; Jacob, C. R.; Hoffmann-Vogel, R. Epitaxial Growth of Pentacene on Alkali Halide Surfaces Studied by Kelvin Probe Force Microscopy. *ACS Nano* **2014**, *8*, 3294–3301.
- (22) Yurtsever, A.; Sugimoto, Y.; Fukumoto, M.; Abe, M.; Morita, S. Effect of Tip Polarity on Kelvin Probe Force Microscopy Images of Thin Insulator CaF₂ Films on Si(111). *Appl. Phys. Lett.* **2012**, *101*, 083119.
- (23) Horcas, I.; Fernández, R.; Gómez-Rodríguez, J.; Colchero, J.; Gómez-Herrero, J.; Baro, A. WSXM: A Software for Scanning Probe Microscopy and a Tool for Nanotechnology. *Rev. Sci. Instrum.* **2007**, *78*, 013705.
- (24) Bikondoa, O.; Pang, C. L.; Ithnin, R.; Muryn, C. A.; Onishi, H.; Thornton, G. Direct Visualization of Defect-Mediated Dissociation of Water on TiO₂(110). *Nat. Mater.* **2006**, *5*, 189–190.
- (25) Wendt, S.; Matthiesen, J.; Schaub, R.; Vestergaard, E. K.; Laegsgaard, E.; Besenbacher, F.; Hammer, B. Formation and Splitting of Paired Hydroxyl Groups on Reduced TiO₂(110). *Phys. Rev. Lett.* **2006**, *96*, 066107.
- (26) Zhang, Z.; Bondarchuk, O.; Kay, B. D.; White, J. M.; Dohnálek, Z. Imaging Water Dissociation on TiO₂(110): Evidence for Inequivalent Geminate OH Groups. *J. Phys. Chem. B* **2006**, *110*, 21840–21845.
- (27) Pang, C. L.; Sasahara, A.; Onishi, H.; Chen, Q.; Thornton, G. Noncontact Atomic Force Microscopy Imaging of Water Dissociation Products on TiO₂(110). *Phys. Rev. B* **2006**, *74*, 073411.
- (28) Lauritsen, J. V.; Foster, A. S.; Olesen, G. H.; Christensen, M. C.; Kühnle, A.; Helveg, S.; Rostrup-Nielsen, J. R.; Clausen, B. S.; Reichling, M.; Besenbacher, F. Chemical Identification of Point Defects and Adsorbates on a Metal Oxide Surface by Atomic Force Microscopy. *Nanotechnology* **2006**, *17*, 3436–3441.
- (29) Enevoldsen, G. H.; Foster, A. S.; Christensen, M. C.; Lauritsen, J. V.; Besenbacher, F. Noncontact Atomic Force Microscopy Studies of Vacancies and Hydroxyls of TiO₂(110): Experiments and Atomistic Simulations. *Phys. Rev. B* **2007**, *76*, 205415.
- (30) Bechstein, R.; González, C.; Schütte, J.; Jelinek, P.; Pérez, R.; Kühnle, A. ‘All-Inclusive’ Imaging of the Rutile TiO₂(110) Surface using NC-AFM. *Nanotechnology* **2009**, *20*, 505703.
- (31) Yurtsever, A.; Sugimoto, Y.; Abe, M.; Morita, S. NC-AFM Imaging of the TiO₂(110)-(1 × 1) Surface at Low Temperature. *Nanotechnology* **2010**, *21*, 165702.
- (32) Yurtsever, A.; Fernández-Torre, D.; González, C.; Jelinek, P.; Pou, P.; Sugimoto, Y.; Abe, M.; Pérez, R.; Morita, S. Understanding Image Contrast Formation in TiO₂ with Force Spectroscopy. *Phys. Rev. B* **2012**, *85*, 125416.
- (33) Batzill, M.; Katsiev, K.; Gaspar, D. J.; Diebold, U. Variations of the Local Electronic Surface Properties of TiO₂(110) Induced by Intrinsic and Extrinsic Defects. *Phys. Rev. B* **2002**, *66*, 235401.

- (34) Uetsuka, H.; Pang, C.; Sasahara, A.; Onishi, H. Photochemical Reaction of Trimethyl Acetate on Pt/TiO₂(110). *Langmuir* **2005**, *21*, 11802–11805.
- (35) Pang, C. L.; Lindsay, R.; Thornton, G. Structure of Clean and Adsorbate-Covered Single-Crystal Rutile TiO₂ Surfaces. *Chem. Rev.* **2013**, *113*, 3887–2948.
- (36) Henderson, M. A.; Lyubinetsky, I. Molecular-Level Insights into Photocatalysis from Scanning Probe Microscopy Studies on TiO₂(110). *Chem. Rev.* **2013**, *113*, 4428–4455.
- (37) Ebert, Ph. Nano-Scale Properties of Defects in Compound Semiconductor Surfaces. *Surf. Sci. Rep.* **1999**, *33*, 121–303.
- (38) Zheng, J. F.; Liu, X.; Newman, N.; Weber, E. R.; Ogletree, D. F.; Salmeron, M. Scanning Tunneling Microscopy Studies of Si Donors (Si_{Ga}) in GaAs. *Phys. Rev. Lett.* **1994**, *72*, 1490–1493.
- (39) Domke, C.; Ebert, Ph.; Heinrich, M.; Urban, K. Microscopic Identification of the Compensation Mechanisms in Si-Doped GaAs. *Phys. Rev. B* **1996**, *54*, 10288–10291.
- (40) Diebold, U.; Koplitz, L. V.; Dulub, O. Atomic-Scale Properties of Low-Index ZnO Surfaces. *Appl. Surf. Sci.* **2004**, *237*, 336–342.
- (41) Zheng, H.; Weismann, A.; Berndt, R. Manipulation of Subsurface Donors in ZnO. *Phys. Rev. Lett.* **2013**, *110*, 226101.
- (42) Cui, Y.; Nilius, N.; Freund, H.-J.; Prada, S.; Giordano, L.; Pacchioni, G. Controlling the Charge State of Single Mo Dopants in a CaO Film. *Phys. Rev. B* **2013**, *88*, 205421.
- (43) Byl, O.; Yates, J. T., Jr. Anisotropy in the Electrical Conductivity of Rutile TiO₂ in the (110) Plane. *J. Phys. Chem. B* **2006**, *110*, 22966–22967.
- (44) Li, S. C.; Zhang, Z.; Sheppard, D.; Kay, B. D.; White, J. M.; Du, Y.; Lyubinetsky, I.; Henkelman, G.; Dohnálek, Z. Intrinsic Diffusion of Hydrogen on Rutile TiO₂(110). *J. Am. Chem. Soc.* **2008**, *130*, 9080–9088.
- (45) Yim, C. M.; Pang, C. L.; Thornton, G. Oxygen Vacancy Origin of the Surface Band-Gap State of TiO₂(110). *Phys. Rev. Lett.* **2010**, *104*, 036806.
- (46) Hebenstreit, E. L. D.; Hebenstreit, W.; Giesler, H.; Ventrice, C. A., Jr.; Hite, D. A.; Sprunger, P. T.; Diebold, U. The Adsorption of Chlorine on TiO₂(110) Studied with Scanning Tunneling Microscopy and Photoemission Spectroscopy. *Surf. Sci.* **2002**, *505*, 336–348.
- (47) Mao, X.; Lang, X.; Wang, Z.; Hao, Q.; Wen, B.; Ren, Z.; Dai, D.; Zhou, C.; Liu, L.-M.; Yang, X. Band-Gap States of TiO₂(110): Major Contribution from Surface Defects. *J. Phys. Chem. Lett.* **2013**, *4*, 3839–3844.
- (48) Ishibashi, T.; Uetsuka, H.; Onishi, H. An Ordered Retinoate Monolayer Prepared on Rutile TiO₂(110). *J. Phys. Chem. B* **2004**, *108*, 17166–17170.
- (49) Kinoshita, K.; Suzuki, S.; Chun, W. J.; Takakusagi, S.; Asakura, K. Adsorption Structure of Acetic Anhydride on a TiO₂(110) Surface Observed by Scanning Tunneling Microscopy. *Surf. Sci.* **2009**, *603*, 552–557.